Fuel 138 (2014) 176–182

Contents lists available at ScienceDirect

Fuel

journal homepage: www.elsevier.com/locate/fuel

Estimation of overall heat transfer coefficients in packed beds with cocurrent downflow of gas and liquid

María J. Taulamet, Néstor J. Mariani, Guillermo F. Barreto, Osvaldo M. Martínez *

PROIRQ, Departamento de Ingeniería Química, Facultad de Ingeniería, UNLP, La Plata, Argentina
Centro de Investigación y Desarrollo en Ciencias Aplicadas "Dr. J. J. Ronco" (CINDECA), CCT La Plata-CONICET-UNLP, Calle 47 No. 257, CP B1900AJK, La Plata, Argentina

HIGHLIGHTS

- Heat transfer between a trickle bed reactor and heating fluid was studied.
- Experiments with different pellet shapes were carried out.
- A suitable correlation for an overall heat transfer coefficient was reported.

ARTICLE INFO

Article history:
Received 16 March 2014
Received in revised form 21 July 2014
Accepted 22 July 2014
Available online 2 August 2014

Keywords:
Trickle bed reactors
Overall heat transfer rates
One-dimensional pseudohomogeneous model

ABSTRACT

This contribution undertakes the analysis of heat transfer between a packed bed with cocurrent downflow of gas and liquid, widely known as trickle bed reactor, and an external heating or cooling fluid. Experiments were carried out in a bench scale reactor with water and air, covering trickle and pulsing regimes, in beds presenting aspect ratios (tube to particle diameter ratio) from 4.7 to 34. Four sizes of glass spheres, two of glass cylinders, a mixture of spheres and a commercial trilobe pellet were employed as particles. With the purpose of estimating the overall heat transfer rates, a 1D pseudo-homogeneous model with a single parameter (overall bed heat transfer coefficient, h_T) was employed to analyze the experimental results. An expression to estimate h_T (expressed as Nusselt number) for the low interaction regime in terms of liquid Reynolds number, a pellet shape factor and bed to particle diameter ratio is proposed. This expression approximates the experimental values with an average deviation of around 10%.

1. Introduction

Trickle-bed reactors (TBR) have been widely employed for years in petroleum, petrochemical and chemical plants [1]. In addition, new applications in biochemical and electrochemical processes and effluent treatment have arisen in recent years [2].

The simulation of these units is far from being carried out confidently due to the uncertainties introduced by the complex fluid-dynamic behavior, which has a noticeable effect on heat and mass transport processes.

In several applications, such as MIBK (methyl isobutyl ketone) synthesis and conversion of natural gas to liquid hydrocarbons by Fischer–Tropsch synthesis [3,4], it is necessary to exchange heat with an external fluid by using multi-tubular TBR. Heat transfer also plays a relevant role in laboratory and bench scale TBR, when studying catalyst performance or in the development of new processes. In such cases, it is commonly desirable to operate under isothermal conditions to facilitate the interpretation of the experimental data [1]. Then, it is essential to correctly evaluate beforehand the overall heat transfer capacity of the bed.

Aiming at estimating the overall heat transfer rates in TBR, two different approaches can be followed. On one hand, the two-dimensional pseudo-homogenous model (2DPH) accounting for radial and axial temperature distributions can be employed [5–13]. The 2DPH model introduces two thermal parameters, the radial effective thermal conductivity (k_{er}) and the wall heat transfer coefficient (h_w). About ten correlations to estimate k_{er} are available in the literature, but reliable predictions can only be reached for air and water flow through beds of spherical particles. Just a few studies have involved cylindrical particles and k_{er} estimation from the proposed correlations is noticeably scattered. No experimental data are available for multi-lobular pellets, up to the best of our knowledge [14]. Concerning coefficient h_w, an even worst scenario is found. The available literature correlations for h_w present deviations larger than 100%, even when tested for spherical particles and air–water flow [14]. The difficulty in estimating h_w

* Corresponding author at: PROIRQ, Departamento de Ingeniería Química, Facultad de Ingeniería, UNLP, La Plata, Argentina.
E-mail address: ommartin@ing.unlp.edu.ar (O.M. Martínez).

http://dx.doi.org/10.1016/j.fuel.2014.07.064
0016-2361/

Nomenclature

a	bed aspect ratio d_t/d_{eq} (–)
C_P	specific heat (J kg^{-1} °C^{-1})
d_p	particle diameter (m)
d_{eq}	equivalent diameter (m)
d_t	tube diameter (m)
G	gas superficial mass flowrate (kg m^{-2} s^{-1})
h_c	jacket heat transfer coefficient (W m^{-2} °C^{-1})
h_T	overall heat transfer coefficient in the bed (W m^{-2} °C^{-1})
H	particle length (m)
k	fluid thermal conductivity (W m^{-1} °C^{-1})
L	liquid superficial mass flowrate (kg m^{-2} s^{-1})
Nu_T	overall Nusselt number, $h_T d_{eq}/k_L$ (–)
Pr	Prandtl number $C_P\mu/k$ (–)
Re	Reynolds number Gd_{eq}/μ or Ld_{eq}/μ (–)
R_T	tube radius (m)
T	temperature (K)
ϕ	particle aspect ratio d_p/H (–)
μ	dynamic viscosity (Pa s)

Subscripts

0	bed inlet
c	heating
E	bed exit
G	gas
L	liquid

stems in the fact that this parameter does not describe a single feature, but it encloses a number of effects related to changes in particle packing and fluid flow in the near-wall region, as discussed extensively in [15] for single-phase flow and specifically for TBR in [16]. These effects will be, in particular, revealed for beds of low tube-to-particle diameter ratio (aspect ratio, a). A significant impact of a upon h_w and also, on k_{er} have been found by Mariani et al. [12], although a systematic study is still lacking.

Thus, despite the fact that the 2DPH model is potentially able to cope with axial and radial temperature profiles and hence it can be expected an accurate prediction of the reaction rates for simulation purposes, there is at present a significant shortage of experimental data and correlations to estimate confidently its thermal parameters. In this context, not even a correct estimation of the overall heat transfer rate can be warranted.

The second approach mentioned above to quantify the overall heat transfer rate is the use of the one dimensional pseudohomogeneous (1DPH) model. This simpler alternative only needs one thermal parameter (the overall heat transfer coefficient, h_T). If this parameter can be well estimated, the 1DPH model will predict correctly the overall heat transfer rates to the bed-wall and, consequently, the average axial temperature profile. In many cases involving moderate radial temperature profiles (say up to a few tens of degrees), the rate of reaction will be also suitably estimated based on temperature averaged on the bed cross-section and reliable simulations can be achieved from the 1DPH model. A set of experimental heat transfer measurements performed with spherical particles was analyzed by Mariani et al. [12] according to both 2DPH and 1DPH models, and the resulting values of their respective parameters correlated with operating variables. The h_T correlation could fit satisfactorily the results for the whole range of values of a (from 4.7 to 34), while the h_w expression had to be restrained for $a > 15$ and that of k_{er} for $a > 8$. The average deviation from the h_T correlation was also smaller than the corresponding values for k_{er} and h_w. These results strongly suggest that parameter h_T can be more easily and reliably employed to perform the regression of experimental heat transfer rates in TBR than the 2DPH model's parameters, k_{er} and h_w, particularly for the range of low aspect ratio (say $5 < a < 15$) which is most relevant for multitubular catalytic reactors. A possible reason for this behavior is that the significant impacts that the aspect ratio a exerts individually on k_{er} and h_w become weaker, because of compensating effects, for the global parameter h_T.

Apart from our previous study [12] on spherical particles, we are not aware of further contributions employing the overall heat transfer coefficient h_T to describe the thermal behavior of TBR. Thus, having remarked the usefulness of 1DPH, the main goals of this contribution are to present new experimental results for different particle shapes and to develop a suitable correlation for h_T, accounting for the effect of particle shape, gas and liquid flowrates and bed aspect ratio a.

The experimental data include results for trickling and pulsing regimes in beds of cylinders, spheres of different sizes, a binary mixture of spheres and a commercial trilobe pellet. It should be remarked that in spite of the industrial relevance of trilobe catalytic pellets in commercial hydrotreating units, no experimental heat transfer data employing this pellet shape has been reported in the open literature.

2. Experimental set-up and procedure

The experimental work was carried out using a cylindrical jacketed tube of 51.4 mm of internal diameter, as shown in Fig. 1. Spheres and cylinders of different sizes and a commercial trilobe pellet (a spent catalyst employed in a hydrotreatment process) were used in the experiments. Material and dimensions of the pellets are reported in Table 1. Two aspects deserve additional comments. On one hand, the commercial trilobe pellets have a non-uniform length distribution; therefore, the value reported in Table 1 (6.6 mm) corresponds to the arithmetic mean of a representative sample of 200 pellets. Values between 2.8 and 13.9 mm were measured according to a nearly normal distribution. On the other hand, a binary mixture of spheres of different sizes (2/3 of 6 mm and 1/3 of 7 mm) with an average diameter of 6.3 mm was also employed.

No universally accepted criterion was found in the literature about the characteristic size to be used for heat transfer analysis in the case of non-spherical pellets. The equivalent diameter (d_{eq}) here employed is the one of a sphere that has the same ratio between volume and external surface, the so-called Sauter diameter. The pellet shape for cylinders and trilobes was characterized by the ratio between diameter and length, $\phi = d_p/H$. It is worth clarifying that in the case of the trilobe pellet, d_{eq} was calculated on the basis of the actual pellet cross-section while ϕ was calculated by considering the diameter d_p of the lobes envelope.

Water and air were employed as fluids fed in the bed at atmospheric pressure and room temperature. The liquid superficial mass flowrate was varied from 2.2 to 14.1 kg m^{-2} s^{-1} and the gas superficial mass flowrate from 2.6×10^{-2} to 0.9 kg m^{-2} s^{-1}, covering trickling and pulsing flow regime. Thermo-physical properties of fluids were evaluated at mean temperature (between bed inlet and exit) for each experiment.

The heating fluid was water kept at 80 °C using an electrical heater. It was circulated in a three-section jacket, identified as upper, middle, and lower sections (Fig. 1). The hot water could pass through one, two, or all of the three sections, thus allowing three lengths of active heat transfer surface, 270, 470 and 870 mm.

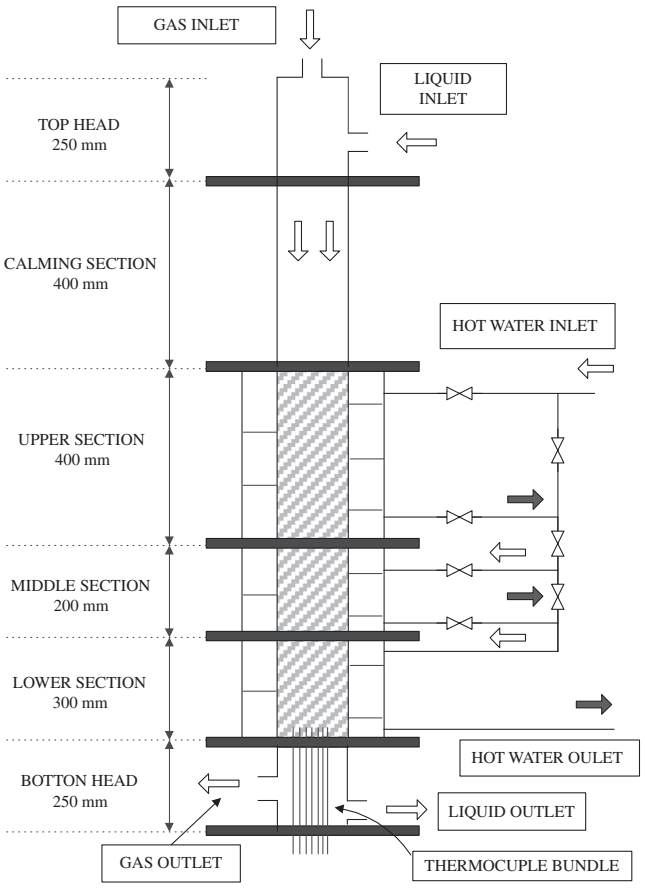

Fig. 1. Sketch of the experimental set-up.

Table 1
Information of particles used in the experiments.

Particle	Material	Size (mm)	d_{eq}	ϕ	a
Spheres 1	Glass	1.5	1.5	1	34.27
Spheres 2		3.0	3.0	1	17.13
Spheres 3		6.0	6.0	1	8.57
Spheres 4		6.3[a]	6.3	1	8.21
Spheres 5		11.0	11.0	1	4.67
Cylinders 1	Glass	d_p = 2 H = 6.5	2.6	0.308	19.77
Cylinders 2		d_p = 8.74 H = 11.8	9.6	0.741	5.35
Trilobes	Porous alumina	d_p = 2.6[b] H = 6.6	2.12[c]	0.394	24.19

[a] Mixed-size sample of spheres of 6 and 7 mm in diameter.
[b] Diameter of the envelope of lobes.
[c] Calculated considering the actual cross-section of the pellet.

The top of the tube (calming section in Fig. 1) was also packed with the same particles employed in the heating zone to provide uniform temperature and flow distributions at the inlet of the jacketed zone.

Temperature was measured at the inlet and outlet of each section of the jacket, at the bed inlet, at the bed outlet in the liquid phase, at nine points distributed radially and angularly over the bed cross section at about 30 mm above the supporting plate of the bed, and at three axial positions within the tube-wall. All temperature readings were recorded by a data acquisition system.

It is worth mentioning that the heating water flowrate was high enough to maintain nearly isothermal conditions within the jacket.

For each experimental condition, defined by a given packing size and shape, liquid and air flowrates and heat transfer length, between 4 and 8 replicates were performed. Before performing each replicate, the bed was fluidized by water to provide different random packings. Each run demanded about 3–4 h. After reaching steady state conditions, the recorded sets of temperatures (about 2000 in each run) were averaged to obtain the values used for analytical purposes.

Some other details concerning the experimental set-up and operating procedure can be found in Mariani [17].

3. Modeling and analysis of experimental results

According to the 1DPH model, the energy balance under the usual hypothesis of steady state operation, no temperature difference between phases, negligible axial thermal conduction, reads:

$$(LC_{PL} + GC^*_{PG})\frac{d\overline{T}}{dz} = \frac{2}{R_T}U(T_c - \overline{T}) \tag{1a}$$

$$\text{at} \quad z = 0, \quad \overline{T} = \overline{T}_0 \tag{1b}$$

where C^*_{PG} is a modified heat capacity that accounts for the partial vaporization of the liquid phase, evaluated as:

$$C^*_{PG} = \frac{\widehat{H}_E - \widehat{H}_0}{\overline{T}_E - \overline{T}_0} \tag{1c}$$

$\widehat{H}_E$ and $\widehat{H}_0$ are the enthalpies of saturated air–steam per unit mass of dry air at the bed-inlet temperature ($\overline{T}_0$) and bed-exit temperature ($\overline{T}_E$), respectively, and T_c is the heating fluid temperature, which is considered to be uniform along the bed length.

In Eq. (1a) the jacket-to-bed heat transfer coefficient U is defined as

$$\frac{1}{U} = \frac{1}{h_T} + \frac{1}{h_c} \tag{2}$$

where h_c is the jacket to wall heat transfer coefficient.

Eq. (1a) can be integrated with the inlet condition (1b) to obtain the averaged temperature at a given axial position z:

$$\overline{T} = T_c - (T_c - \overline{T}_0)\exp\left\{-\frac{2U}{(LC_{PL} + GC^*_{PG})R_T}z\right\} \tag{3}$$

Using measured values of $\overline{T}_0$ and $\overline{T}_E$, the heat transfer coefficient U can be readily calculated from Eq. (3). Eq. (2) allows evaluating h_T, as h_c is known from the work of Mariani [17], who employed the same experimental set-up.

Two issues concerning the experimental measurements are discussed next.

On one hand, the use of several active lengths for heat transfer (*i.e.*, up to three sections of the jacket), allowed confirming that *entrance effects* were not negligible. Consequently, experimental data for the shortest length were not employed in the analysis. In addition, when using the three sections under certain experimental conditions, it was checked that the outlet temperature approached very closely the jacket temperature, and the difference $\overline{T}_E - T_c$ in Eq. (3) could not be evaluated with due accuracy. Therefore, only the data employing two sections (470 mm of active length) were considered for the analysis.

On the other hand, two alternatives were available to evaluate $\overline{T}_E$: the mixing cup temperature of the exit liquid stream and the average temperature from the measured radial temperature profile. If the liquid flow distribution were uniform, both values would match within the experimental error. However, a noticeable and systematic deviation was observed, being the mixing cup temperature higher than the average from the radial profile, particularly, for the larger-sized particles. For cylindrical particles, this difference increases as the liquid flowrate increases. This behavior can

be adequately explained by recalling that the wall of the container induces a highly ordered particle layer contacting the wall. The effect of the wall is attenuated toward the interior of the bed until a virtual random packing is reached at distances of a few particle diameters from the wall [18]. These packing features affect void fraction and radial liquid distributions, leading to higher values of these magnitudes in the neighborhood of the wall. Also, in this region temperature is higher than in the bed core. In turn, this effect will be more noticeable for beds of low aspect ratios *a* (*i.e.*, for particles of larger sizes). Therefore, the mixing cup temperature is the correct measurement to evaluate the heat transfer coefficient, and it was used to this purpose.

4. Results and discussion

4.1. Influence of operating conditions

The effect of liquid and gas superficial mass flowrates (*L* and *G*, respectively) and flow regime on the overall heat transfer coefficient will be analyzed in this section. As regards the effect of flow regime, Fig. 2 shows a flow map intending to discriminate the regime corresponding to each of the experimental data points gathered in this work. The correlation of Larachi et al. [19] has been employed to that purpose. Some boundary points evaluated by us from visual observations are also included.

Experimental results obtained in this study are conclusive in the sense that the main contribution to heat transfer in TBR is the radial convective dispersion of the liquid phase, as expected from the fact that *L* is always significantly greater than *G* (see Section 2). h_T increases as *L* increases, irrespective of the flow regime and the level of G, for all conditions studied in this work. An example can be visualized in Fig. 3 for both cylinder sizes (Table 1).

The effect of gas flowrate *G* is less clearly defined. To provide an explanation, it is necessary to distinguish the flow regime and particle shape. The results for h_T with both cylinder sizes (Table 1) are plotted in Fig. 3, in which different levels of *G* and conditions of either low or high interaction regime are identified. The continuous lines were obtained from the expression proposed and discussed in Section 4.3. The conditions of high interaction regime in Fig. 3 can be separated into two groups. Points (*A*) and (*B*) for d_{eq} = 2.6 mm (also identified in Fig. 2) correspond to the highest values of both *G* and *L*, for which a very intense interaction between fluid phases is expected. The behavior of the remaining

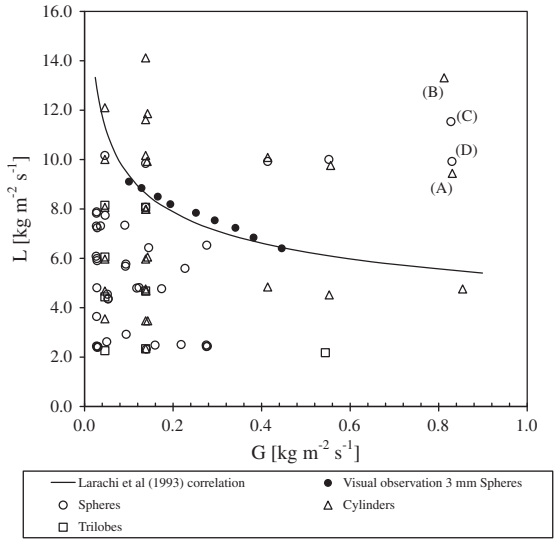

Fig. 2. Flow map including experimental conditions, visual observation of flow regime change and Larachi et al. [19] correlation.

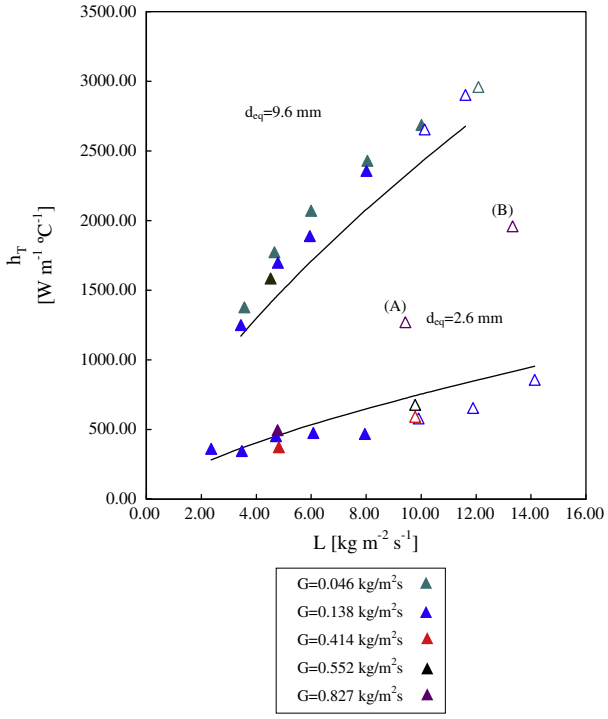

Fig. 3. h_T vs *L* for cylindrical particles (filled symbols are for low interaction regime and empty symbols for high interaction regime). Continuous lines: predictions from Eq. (4).

data points in the high interaction regime does not depart significantly from the set of points in the low interaction regime, and all of them are correctly described by the same correlating curves without including any effect of *G*. It is clear that values of h_T for points *A* and *B* escape from this trend, a fact that can be probably explained by a qualitatively different fluid-dynamics effect, which deserves additional experimental efforts for their quantification.

It is worth mentioning that other correlations for flow regime were tried (*i.e.*, [20,21]) and the conclusions discussed above remain virtually the same.

A similar behavior of h_T with gas flowrate was observed for spherical particles.

Therefore, for monosized spheres and cylinders and for the mixed-size sample of spheres (spheres 4 in Table 1) in low interaction regime no effect of G could be appreciated.

Values of h_T for trilobe particles are plotted in Fig. 4. In this case, all the data points correspond to the low interaction regime (Fig. 2), and it can be observed that, at variance to the behavior of cylinders, higher gas flowrates lead in most instances to higher values of h_T. The continuous curves in Fig. 4 were obtained from the correlation discussed in Section 4.3, which already includes the effect of *G*, specifically for trilobe particles. In spite of this observation, it is important to note that *G* exerts a definitely weaker effect than *L*. No definite explanation has been found for the effect of *G* in this case. A distinction between trilobes and the remaining particles is that the former are made of a porous ceramic (they are catalyst pellets), while the other particles are glass made. The trilobes may then be more prone to retain liquid and therefore to promote higher liquid hold-ups, while the grooves between lobes may also act in the same direction. It is worth mentioning that fluid-dynamics studies [22,23] show that for equivalent operating conditions the liquid hold-up is higher for trilobes than for spheres. Therefore, it can be hypothesized that the gas flowrate can be effective in dragging part of the liquid attached to the trilobe particles.

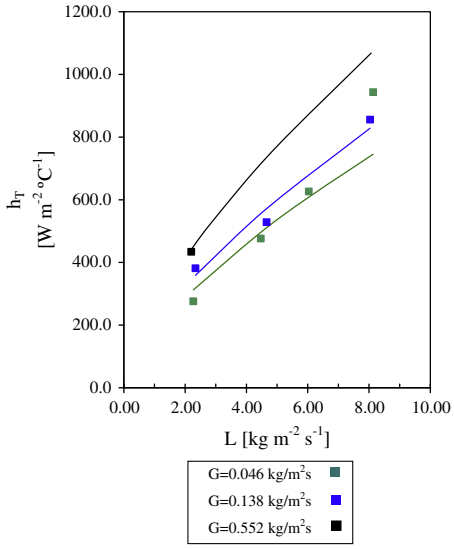

Fig. 4. h_T vs L for trilobe particles. Continuous lines: predictions from Eq. (4).

4.2. Influence of shape and size of the particles

Fig. 5 illustrates the behavior of h_T for some of the packings in Table 1. Continuous curves were plotted from Eq. (4) presented in the next section. The curve for the trilobe pellets in Fig. 5 corresponds to an intermediate value of gas superficial mass flowrate ($G = 0.15$ kg m^{-2} s^{-1}).

For each particle shape studied in this contribution, h_T increases as the equivalent diameter of the particles (d_{eq}) increases. This fact can be visualized in Fig. 5 by comparing the data for Spheres 1 and 5 and those for Cylinders 1 and 2.

The packing of cylinders is known to depend upon the ratio $\phi = d_p/H$. Thus, beds of "long" cylinders ($\phi = 0.308$) show larger voidages than "short" cylinders ($\phi = 0.741$) (see *e.g.* Rase [24]), a fact that reveals that the latter are able to accommodate better. One direct consequence of smaller voidages is that interstitial velocities (for the same L) will be larger, causing lateral dispersion to become more intense. Then, it can be expected that larger values of ϕ will increase h_T. Cylinders 1 and 2 show indeed this effect when compared with spheres of similar sizes. The sizes of Cylinders 2 ($\phi = 0.741$) and Spheres 5 are close to each other ($d_{eq} = 9.6$ mm and 11 mm, respectively) and their values of h_T are alike. Instead, the "long" Cylinders 1 ($\phi = 0.308$) show definitely lower values of h_T than Spheres 1, in spite of presenting a larger d_{eq} (2.6 mm vs. 1.5 mm).

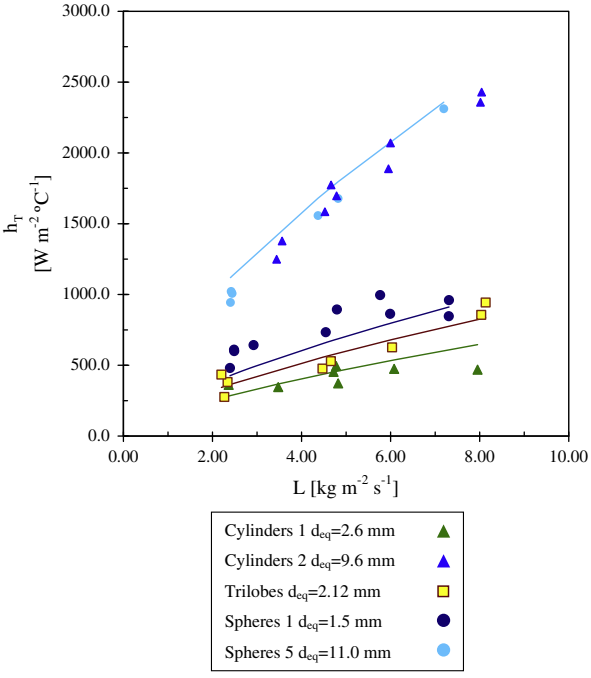

Fig. 5. h_T vs L for different shaped particles. Continuous lines: predictions from Eq. (4).

Regarding the values of h_T for the trilobe pellets in Fig. 5, they lie above those of Cylinders 1 and below those of Spheres 1. This behavior can be adequately interpreted by recalling that ϕ is around of 30% greater for trilobes than for Cylinders 1, while d_{eq} is slightly larger for the latter (2.12 mm vs. 2.6 mm). The same reasoning can be applied for comparing trilobes and Spheres 1.

4.3. Correlation for the overall heat transfer coefficient

From the discussion in previous sections, it can be concluded that a correlation for h_T should include the effects of liquid flowrate, particle size (Sauter diameter) and shape (particle aspect ratio, ϕ). For the specific case of trilobe pellets, the effect of gas flowrate has also been incorporated.

The liquid Prandtl number is most likely to have an effect of h_T. However, as we have only employed water in our experimental program, it has not been included in the proposed correlation.

The following expression has been employed to perform the regression analysis of the experimental data

$$\mathrm{Nu}_T = \frac{h_T d_{eq}}{k_L} = b[1 - \exp(-f\,\phi^n/a)]\,\mathrm{Re}_L^e(1 + h\,\mathrm{Re}_G^g) \tag{4}$$

where b, f, n, e, h and g are fitting parameters, and Re_L and Re_G are calculated using d_{eq} as the characteristic length.

Eq. (4) predicts $\mathrm{Nu}_T = 0$ for a stagnant bed ($\mathrm{Re}_L = 0$). Although in practice, thermal conduction mechanisms will allow a finite Nusselt number, under the present experimental conditions (relatively large values of L) the addition of a constant term Nu_{T0} in Eq. (4) did not show statistical significance.

Parameters of Eq. (4) were obtained by minimizing the objective function,

$$F = \sum_{i=1}^{N}[(\mathrm{Nu}_{T,i}^{pred} - \mathrm{Nu}_{T,i}^{exp})/\mathrm{Nu}_{T,i}^{exp}]^2$$

with $N = 69$ (experimental data of low interaction regime). The optimal values of parameters are:

$$b = 2.51 \quad f = 4.71 \tag{5a, b}$$

$$n = 0.7 \quad e = 0.68 \tag{5c, d}$$

$$h = \begin{cases} 0.05 & \text{(trilobes)} \\ 0 & \text{(spheres, cylinders)} \end{cases} \qquad g = 0.6 \tag{5e, f}$$

The average relative deviation of Eq. (4), defined by

$$E = \frac{1}{N}\sum_{i=1}^{N}\left|(\mathrm{Nu}_T^{pred} - \mathrm{Nu}_T^{exp})/\mathrm{Nu}_T^{exp}\right|$$

is 10.9%, with a maximum deviation of 28%. The error distribution is very reasonably balanced, with 32 negative and 37 positive values. Figs. 3–5 allow appreciating the goodness of fit for the different particles sizes and shapes. In addition, a parity plot between experimental and predicted Nu_T is presented in Fig. 6 for all particles included in Table 1.

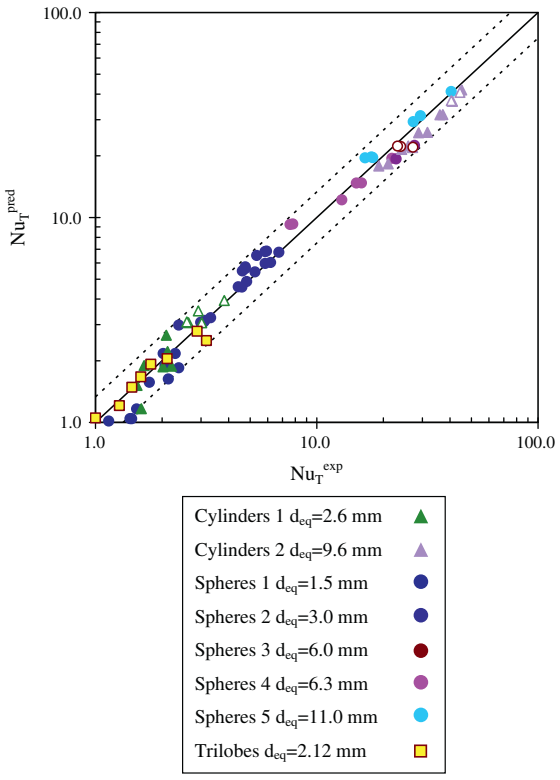

Fig. 6. Parity plot experimental and predicted (Eq. (4)) Nu_T (filled symbols are for low interaction regime and empty symbols for high interaction regime).

The experimental data employed to fit Eq. (4) were those corresponding to the low interaction regime (Fig. 2). Accordingly, the ranges covered in this investigation are $a > 4.7$ and $5.4 < Re_L < 170$. However, it is interesting to explore the predictive ability of Eq. (4) in the high interaction regime, as it was already discussed that values of h_T seem to follow the trend of the low interaction regime (Fig. 3), provided that conditions do not depart much from the boundary between both regions (Fig. 2). The experimental results of h_T in the high interaction regime are included in Fig. 6 (excluding those for conditions *A*, *B*, *C*, *D* in Fig. 2, *i.e.* those strongly departing from the transition line), where it can be appreciated that these data points are very well approximated by the estimations from Eq. (4). It can be concluded that Eq. (4) can also be useful at operating conditions in the high interaction regime lying not too far from the transition boundary.

5. Conclusions

Results from an experimental investigation on heat transfer from a packed bed with cocurrent gas–liquid downflow to the wall have been presented. The measurements cover the range of operating liquid and gas flowrates of the trickle and pulsing regime in beds of aspect ratios (tube to particle diameter ratio) from 4.7 to 34. Glass spheres of four different sizes and a mixed-size sample, two glass cylinder particles and a commercial trilobe catalyst pellet were used in the experiments. Up to the best of our knowledge, there is no previous study reporting heat transfer measurements in beds packed with trilobe particles.

Aiming to predict overall heat transfer rates, a one-dimensional pseudo-homogeneous model, presenting a single thermal parameter (h_T), has been employed to process the experimental data. The analysis of the behavior of h_T allows drawing some useful conclusions to propose a correlation for predictive purposes. In first place, the main contribution to heat transfer is the radial convective dispersion of the liquid phase, due to the relatively higher values of liquid superficial mass flowrate (L) as compared with gas superficial mass flowrate (G). Accordingly, as L increases h_T always increases, no matter which flow regime or particle shape is being considering. In addition, keeping all the remaining variables unchanged, the lower the aspect ratio the higher the heat transfer rates. On the contrary, the effect of G is not as clear as that of L. While for cylinders and spheres in low interaction regime G shows no significant effect, a weak but definite impact was observed for trilobes: the higher the value of G, the higher the value of h_T. Finally, the effect of particle size was correctly accounted for by the Sauter diameter (the diameter of a sphere showing the same volume to external surface ratio, d_{eq}) and the effect of shape could be adequately quantified by using the particle aspect ratio $\phi = d_p/H$.

A single expression proposed to estimate h_T, Eq. (4), was able to fit the whole set of experimental data, including all particle shapes and a large range of bed-to-particle diameter ratios, $4.7 < a < 34$, which widely covers values likely to be found in full scale multitubular TBR. Relative average deviation between predicted and measures values of h_T is 10.9%.

Acknowledgements

The authors wish to thank the financial support of the following argentine institutions: ANPCyT-SECyT (PICT # 1641), CONICET (PIP # 0304) and UNLP (PID # 11/I177). N.J.M., O.M.M. and G.F.B. are Research Members of CONICET and M.J.T. holds a fellowship from CONICET.

References

[1] Ancheyta J. Modeling and simulation of catalytic reactors for petroleum refining. New Jersey: J. Wiley & Sons Inc.; 2011.
[2] Ranade VV, Chaudhari RV, Gunjal PR. Trickle bed reactors – reactor engineering and applications. Oxford: Elsevier; 2011.
[3] Krishna R, Sie ST. Strategies for multiphase reactor selection. Chem Eng Sci 1994;49:4029–65.
[4] Zhu X. A study of radial heat transfer in fixed bed Fischer-Tropsch synthesis reactors. PhD Dissertation, University of the Witwatersrand; 2013.
[5] Hashimoto K, Murayoma K, Nagata S, Fujiyoshi K. Effective radial thermal conductivity in concurrent flow of gas and liquid through packed bed. Kagaku Kogaku Ronbunshu 1976;2:53–9.
[6] Murayoma K, Hashimoto K, Tomita T. Heat transfer from the wall in gas–liquid concurrent packed beds. Kagaku Kogaku Ronbunshu 1977;3:612–6.
[7] Matsuura A, Hitaka Y, Akehata T, Shirai T. Apparent wall heat transfer coefficient in packed beds with downward concurrent gas–liquid flow. Kagaku Kogaku Ronbunshu 1979;5:263–8.
[8] Matsuura A, Hitaka Y, Akehata T, Shirai T. Effective radial thermal conductivity in packed beds with gas–liquid downflow. Kagaku Kogaku Ronbunshu 1979;5:269–74.
[9] Specchia V, Baldi G. Heat transfer in trickle-bed reactors. Chem Eng Commun 1979;3:483–99.
[10] Lamine AS, Gerth L, Le Gall H, Wild G. Heat transfer in a packed bed reactor with cocurrent downflow of a gas and a liquid. Chem Eng Sci 1996;51:3813–27.
[11] Babu BV, Sastry KKN. Estimation of heat transfer parameters in a trickle-bed reactor using differential evolution and orthogonal collocation. Comput Chem Eng 1999;23:327–39.
[12] Mariani NJ, Martínez OM, Barreto GF. Evaluation of heat transfer parameters in packed beds with cocurrent downflow of liquid and gas. Chem Eng Sci 2001;56:5995–6001.
[13] Pinto Moreira MF. Avaliação de aspectos fluidodinâmicos e da transferência de calor em leito fixo com escoamento gás–líquido concurrente vertical. Tesis Doctoral, Universidad Federal de São Carlos; 2004.
[14] Taulament MJ, Mariani NJ, Barreto GF, Martínez OM. A critical review on heat transfer in trickle bed reactors. 2014 [submitted for publication]
[15] Dixon AG. Fixed bed catalytic reactor modeling - the radial heat transfer problem. Can J Chem Eng 2012;90:505–27.
[16] Mariani NJ, Mazza GD, Martínez OM, Cukierman AL, Barreto GF. On the influence of liquid distribution on heat transfer parameters in trickle bed systems. Can J Chem Eng 2003;81:814–20.
[17] Mariani NJ. Transferencia de calor en sistemas multifásicos, Tesis Doctoral, Universidad Nacional de La Plata; 2000.
[18] Mariani NJ, Mazza GD, Martínez OM, Barreto GF. The distribution of particles in cylindrical packed beds. Trend Heat Mass Momentum Transfer 1998;4:95–114.

[19] Larachi F, Laurent A, Wild G, Midoux N. Effet de la pression sur la transition ruisselant-pulsé dans le réacteurs catalitiques à lit fixe arrosé. Can J Chem Eng 1993;71:319–21.
[20] Charpentier JC, Favier M. Some liquid holdup experimental data in trickle-bed reactors for foaming and nonfoaming hydrocarbons. AIChE J 1975;21(6):1213–8.
[21] Tosun G. A study of concurrent downflow of nonfoaming system in packed beds. 1. flow regimen: search for a generalized flow map. Ind Eng Chem Process Des Device 1984;23:29–35.
[22] Bazmi M, Hashemabadi SH, Bayat M. Extrudate trilobe catalysts and loading effects on pressure drop and dynamic liquid holdup in porous media of trickle bed reactors. Transport Porous Med 2013;99:535–53.
[23] Nguyen NL. Analysis of the influence of the hydrodynamics in hydrotreating of diesel oil in trickle bed reactors via MRI-measurements. PhD Dissertation, Karlsruhe Institute of Technology; 2011.
[24] Rase HF. Fixed-bed reactor design and diagnostics. Stoneham: Butterworths Publishers; 1990.